17th AIAA/CEAS Aeroacoustics Conference (32nd AIAA Aeroacoustics Conference)
05 - 08 June 2011, Portland, Oregon

AIAA 2011-2836

A further step towards grid-converged solutions for an initially nominally turbulent jet

Christophe Bogey[*], **Olivier Marsden**[†] and **Christophe Bailly**[‡]

Laboratoire de Mécanique des Fluides et d'Acoustique

UMR CNRS 5509, Ecole Centrale de Lyon

69134 Ecully, France

This paper presents the continuation of an earlier work[1] dealing with Large-Eddy Simulations (LES) of a Mach number 0.9 isothermal round jet at a Reynolds number of 10^5, whose boundary layers are tripped inside a pipe nozzle so as to exhibit, at the pipe exit, a laminar mean velocity profile of momentum thickness $\delta_\theta(0) = 0.018$ times the jet radius and peak turbulent intensities around 9%. In order to further assess the validity of the flow and acoustic fields determined by LES, an additional simulation is performed using a finer grid, characterized by minimum mesh spacings of 0.20, 0.34 and 0.40 times $\delta_\theta(0)$, respectively, in the radial, azimuthal and axial directions. The results are compared to previous LES results, as well as to those obtained using the same grid for a jet with identical exit conditions, except for a double boundary-layer thickness, up to 8 radii downstream of the nozzle exit. The new simulation at higher resolution is shown to provide shear-layer solutions that are practically grid-converged and, more generally, numerically accurate and physically relevant[2] data for the present initially nominally turbulent jet, which could serve in future studies.[3]

I. Introduction

Thanks to the growth of computing power as well as to the use of highly accurate methods in compressible Navier-Stokes simulations,[4–6] it appears now possible to compute the flow and acoustic fields of laboratory-scale jets. These jets are at diameter-based Reynolds numbers typically around 10^5, which are in between low and high Reynolds number values. Consequently their initial state is usually transitional, that is neither fully laminar nor fully turbulent. In particular, the peak turbulence intensities at the nozzle-exit section of these jets are likely to significantly vary, which has been found to strongly affect[7–13] their aerodynamic development as well as their far-field noise. Numerical simulations have now to show that they are capable of properly taking into account this influence of the initial conditions on jet features,[14,15] which will demonstrate that they are reliable and provide dependable, physically-based solutions.

With this aim in view, we recently simulated isothermal round jets at Mach number 0.9 and Reynolds number 10^5, with different inflow conditions. In a first step, initially laminar jets[16] were considered. Their initial turbulent development was shown to be dominated by pairings of coherent vortices. In a second step, initially nominally turbulent jets[1] were calculated. Following an approach widely employed in experiments from the seventies[7,8,17,18] to nowadays,[19] the jet boundary layers were tripped in order to generate high initial flow disturbances. More precisely, laminar Blasius mean velocity profiles of momentum thickness $\delta_\theta(0) = 0.018 r_0$ and peak axial turbulent intensities $u'_e \simeq 0.09 u_j$ were specified at the exit of a pipe nozzle, where r_0 and u_j are the pipe radius and the jet velocity, in agreement with the initial conditions in tripped jets of Zaman.[11,12] Two methods of boundary-layer tripping, and four meshes containing from 50 to 252 millions points were used. The jet flow and acoustic fields were found to vary negligibly with the tripping procedure, but appreciably with the grid resolution. The simulation at highest resolution, referred to as

[*]CNRS Research Scientist, AIAA Member, christophe.bogey@ec-lyon.fr

[†]Assistant Professor at Ecole Centrale de Lyon, AIAA Member, olivier.marsden@ec-lyon.fr

[‡]Professor at Ecole Centrale de Lyon & Institut Universitaire de France, Senior AIAA Member, christophe.bailly@ec-lyon.fr

Jetring1024dz, was specially carried out using a grid with minimum mesh spacings Δr, $r_0\Delta\theta$ and Δz in the radial, azimuthal and axial directions, respectively, of 0.72%, 0.61% and 0.72% of the jet radius, that are also equal to 0.40, 0.34 and 0.40 times $\delta_\theta(0)$. This LES provided mean and turbulent jet flow fields comparing well with experimental data for jets at high Reynolds numbers. As for the jet far-field noise, a component typically associated with coherent vortex pairings in the mixing layers was observed, yielding a hump in the sound spectra around 2 dB above the levels measured for jets at Reynolds number $\mathrm{Re}_D \geq 5 \times 10^5$.

In the present paper, the grid convergence of the solutions obtained for the initially nominally turbulent jet at Mach and Reynolds numbers 0.9 and 10^5 considered in the above-mentioned work is further examined. Two additional jet simulations[2] are performed using our in-house LES solver based on low-dissipation finite differences and high-order relaxation filtering. In the first case, referred to as Jetring1024drdz, the jet is computed using a 252 million point grid similar to the grid of Jetring1024dz in the axial and azimuthal directions, but twice as fine in the radial direction along the nozzle-lip line. In the second case, the grid used is that of Jetring1024drdz, up to $z = 8r_0$ in the axial direction, and the pipe-exit flow conditions are $\delta_\theta(0) = 0.036r_0$ and $u'_e = 0.09u_j$. The initial shear layer is thus twice as thick while containing the same amount of velocity fluctuations as previously. The jet Mach number remains 0.9, but the diameter-based Reynolds number is now equal to 5×10^4 in order not to change the Reynolds number based on the exit boundary-layer momentum thickness $\mathrm{Re}_\theta = 900$. Therefore the shear layer is here identical to that in Jetring1024drdz, but the computation is performed at twice the resolution. The results from the two supplementary simulations will be compared to those obtained in the previous simulations, as well as to experimental data when possible. It can finally be emphasized that this work is carried out in order to assess the numerical accuracy and the physical relevance of the jet LES solutions, which could then serve as reference solutions in future studies.[3]

The paper is organized as follows. The jet exit conditions, the numerical methods, the parameters of the LES simulations, and of the method used to propagate the LES near field to the far field are presented in section II. The main features of the initial turbulence just downstream of the nozzle lip, of the shear-layer and jet flow developments and of the far acoustic fields are shown in section III. Concluding remarks are given in section IV.

II. Simulation parameters

A. LES procedure

The simulations are carried out using an in-house solver of the 3-D filtered compressible Navier-Stokes equations in cylindrical coordinates (r, θ, z) using low-dissipation and low-dispersion finite differences. The axis singularity is taken into account by the method of Mohseni and Colonius.[20] Fourth-order eleven-point centered finite differences are used for spatial discretization, and a second-order six-stage low-storage Runge-Kutta algorithm is implemented for time integration.[21] To circumvent the time-step restriction induced by the cylindrical coordinates, the derivatives in the azimuthal direction around the axis are calculated using every n-th grid point, from $n = 2$ up to $n = 32$ or $n = 64$ near the centerline, depending on the azimuthal resolution.[22] A sixth-order eleven-point centered filter designed to damp mainly the shortest waves discretized[23] is applied every time step to the flow variables. The discretization at the boundaries is performed by non-centered finite differences and filters.[16,24] The filtering is also employed to dissipate subgrid-scale energy without significantly affecting the accurately resolved scales.[25] This approach was developed to avoid artificially decreasing the effective flow Reynolds number.[26] More details on the LES approach based on relaxation filtering, referred to as LES-RF, are available in another paper.[27] Finally, in order to minimize wave reflections, radiation conditions[28,29] are specified at the mesh grid boundaries with the addition of a sponge zone at the outflow.

B. Jet definition

In this paper, the results obtained for an isothermal round jet at Mach number $\mathrm{M} = u_j/c_a = 0.9$ and Reynolds number $\mathrm{Re}_D = u_j D/\nu = 10^5$ in two previous LES,[1] Jetring512 and Jetring1024dz, and in the new simulation Jetring1024drdz at higher resolution are presented (u_j is the jet inflow velocity, c_a is the speed of sound in the ambient medium, $D = 2r_0$ is the nozzle diameter, and ν is the kinematic molecular viscosity). The jet originates from a pipe nozzle of radius r_0 and length $2r_0$, including a $0.053r_0$ wide lip. At the pipe inlet at $z = -2r_0$, laminar Blasius boundary-layer profiles of thickness $\delta = 0.15r_0$, or equally

of momentum thickness $\delta_\theta = 0.018r_0$ yielding $\mathrm{Re}_\theta = u_j\delta_\theta/\nu = 900$, are imposed for the axial velocity. Radial and azimuthal velocities are initially set to zero, pressure is kept constant at its ambient value, and the temperature is determined by a Crocco-Busemann relation. The boundary layers are tripped inside the pipe at $z \simeq -r_0$ by adding low-amplitude random velocity fluctuations based on vortical disturbances, decorrelated in the azimuthal direction.[2] The tripping magnitudes are chosen to obtain peak turbulence intensities $u'_e \simeq 0.09u_j$ at the pipe exit in all simulations.

In order to study the grid convergence of the results, an additional jet, referred to as Jetring1024drdz2δ_θ, is considered. In this case, a laminar boundary layer of thickness $\delta_\theta = 0.036r_0$, that is twice the thickness in previous cases, is imposed inside the pipe, and the same tripping procedure is applied to achieve $u'_e \simeq 0.09u_j$. The jet Mach number is still M = 0.9, but its Reynolds number is now $\mathrm{Re}_D = 5 \times 10^4$ in order to keep $\mathrm{Re}_\theta = 900$. The initial shear-layer properties in Jetring1024drdz2δ_θ, namely M, Re_θ and u'_e/u_j, are therefore similar to those in the other jets.

The profiles of mean and rms axial velocities obtained at the pipe exit in the different jets are presented in figure 1. The mean-velocity profiles do not differ appreciably from the Blasius profiles fixed at the pipe inlet, leading to exit boundary-layer momentum thicknesses $\delta_\theta(0) = 0.018r_0$ in Jetring512, Jetring1024dz and Jetring1024drdz, and $\delta_\theta(0) = 0.036r_0$ in Jetring1024drdz2δ_θ. The peak levels of velocity fluctuations are also around 9% of the jet velocity, as desired. The present jets are consequently all initially nominally turbulent. Focusing on the jets with $\delta_\theta(0) = 0.018r_0$, their initial conditions are shown to be comparable to those measured by Zaman[11,12] in tripped jets, including a jet at $\mathrm{Re}_D = 10^5$.

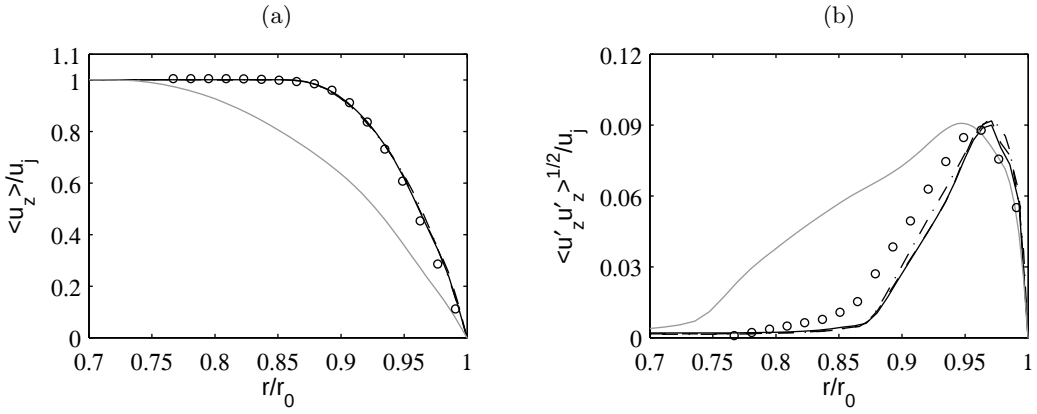

Figure 1. Profiles at $z = 0$ (a) of mean axial velocity $< u_z >$, and (b) of the rms values of fluctuating axial velocity u'_z for ——— Jetring512, − − − Jetring1024dz, − · − · Jetring1024drdz, ——— Jetring1024drdz2δ_θ. Measurements for a Mach 0.18, tripped jet at $\mathrm{Re}_D = 10^5$: ∘ Zaman.[11,12]

C. Simulation parameters

The main parameters of the jet LES are provided in table 1. In the azimuthal direction, the grids are uniform, and contain 512 points in Jetring512, and 1024 points in Jetring1024dz and Jetring1024drdz, giving $r_0\Delta\theta = 0.0061r_0$. In the latter simulations, they are also characterized by $\Delta z = 0.0072r_0$ in the axial direction at $z = 0$, but $\Delta r = 0.0072r_0$ in Jetring1024dz whereas $\Delta r = 0.0036r_0$ in Jetring1024drdz in the radial direction at $r = r_0$. The physical domains, excluding the eighty-point outflow sponge zones, extend axially up to $z = 25r_0$, and radially up to $r = 11r_0$ in Jetring512 and Jetring1024dz, and $r = 9r_0$ in Jetring1024drdz. More information on the mesh grids can be found in a recent paper.[2]

Concerning the discretization of the initial shear layer of momentum thickness $\delta_\theta(0)$, it can be noted that the mesh size in the radial direction at $r = r_0$ is $\Delta r = 0.40\delta_\theta(0)$ in Jetring512 and Jetring1024dz and $\Delta r = 0.20\delta_\theta(0)$ in Jetring1024drdz. In the same way, one gets $r_0\Delta\theta = 0.68\delta_\theta(0)$ using $n_\theta = 512$ and $r_0\Delta\theta = 0.34\delta_\theta(0)$ using $n_\theta = 1024$ in the azimuthal direction, as well as $\Delta z = 0.80\delta_\theta(0)$ in Jetring512 and $\Delta z = 0.40\delta_\theta(0)$ in Jetring1024dz and Jetring1024drdz in the axial direction at $z = 0$.

The numbers of time steps n_t and the non-dimensional times Tu_j/D in Jetring512, Jetring1024dz and Jetring1024drdz are provided in table 1. Between 81,000 and 164,000 iterations are done, corresponding to physical times between $375r_0/u_j$ to $475r_0/u_j$. To study jet features and perform far-field extrapolation, density, velocity components and pressure are recorded from $t = 125r_0/u_j$ at $r = 0$, $r = r_0$ and $r = r_c = 7.25r_0$ ($t = 100r_0/u_j$ and $r_c = 6.5r_0$ in Jetring1024drdz), at a sampling frequency allowing the computation

of spectra up to a Strouhal number 20. The velocity spectra are evaluated from overlapping samples of duration $27.4r_0/u_j$. The flow statistics are determined from $t = 175r_0/u_j$, and they are averaged in the azimuthal direction.

Some parameters of the simulation Jetring1024drdz2δ_θ of a jet with a double initial shear-layer thickness are also given in table 1. The grid used is that of Jetring1024drdz limited axially to $z = 8r_0$. The computation of the mixing layer is thus performed in this case at twice the resolution. Due to the shear-layer thickening, one indeed obtains, at the nozzle lip, $(\Delta r, r_0\Delta\theta, \Delta z) = (0.20, 0.34, 0.40) \times \delta_\theta(0)$ in Jetring1024drdz, but $(\Delta r, r_0\Delta\theta, \Delta z) = (0.10, 0.17, 0.20) \times \delta_\theta(0)$ in Jetring1024drdz2δ_θ.

Table 1. Simulation parameters: exit boundary-layer momentum thickness $\delta_\theta(0)$, numbers of grid points (n_r, n_θ, n_z), mesh spacings Δr at $r = r_0$, $r_0\Delta\theta$, and Δz at $z = 0$, number of time steps n_t, and time duration T.

	$\delta_\theta(0)/r_0$	$n_r \times n_\theta \times n_z$	$\Delta r/r_0$	$r_0\Delta\theta/r_0$	$\Delta z/r_0$	n_t	Tu_j/r_0
Jetring512	1.8%	$256 \times 512 \times 654$	0.72%	1.23%	1.45%	81,000	475
Jetring1024dz	1.8%	$256 \times 1024 \times 962$	0.72%	0.61%	0.72%	95,600	437.5
Jetring1024drdz	1.8%	$256 \times 1024 \times 962$	0.36%	0.61%	0.72%	164,200	375
Jetring1024drdz2δ_θ	3.6%	$256 \times 1024 \times 687$	0.36%	0.61%	0.72%	76,500	175

D. Far-field extrapolation

The LES near fields are propagated to the far field using the wave-extrapolation method developed in recent work,[16,30] by solving the linear acoustic equations in cylindrical coordinates. The numerical schemes and boundary conditions used are those of the LES. Non-centered finite differences and filters are applied at the inner-side boundary of the extrapolation grid. In practice, the extrapolation is performed from fluctuating velocities and pressure recorded in the LES from $t = 125r_0/u_j$ on the surface at $r = r_c = 7.25r_0$ ($t = 100r_0/u_j$ and $r_c = 6.5r_0$ in Jetring1024drdz), at a frequency allowing the computation of spectra up to Strouhal number 20. These data are interpolated onto a cylindrical surface discretized by a uniform mesh spacing $\Delta z = 0.065r_0$ in the axial direction. They are then imposed at the bottom boundary of a grid of $n_r \times n_\theta \times n_z = 835 \times 256 \times 1155$ points ($n_r = 845$ in Jetring1024drdz), extending axially from $z = -16.6r_0$ to $z = 58.2r_0$ and radially up to $r = 61.4r_0$, on which the linear acoustic equations are solved. The grid mesh spacings are uniform with $\Delta r = \Delta z = 0.065r_0$, yielding Strouhal number $\mathrm{St}_D = 8.6$ for four points per wavelength. After a propagation time of $t = 60r_0/u_j$, pressure is recorded at a distance of $60r_0$ from the nozzle-pipe exit, during periods of $300r_0/u_j$ for Jetring512, $290r_0/u_j$ for Jetring1024dz, and $250r_0/u_j$ for Jetring1024drdz. Pressure spectra are then evaluated using overlapping samples of duration $38r_0/u_j$, and they are averaged in the azimuthal direction.

III. Results

The influence of the grid resolution on the flow and acoustic fields of the tripped jet is studied by comparing the results obtained from the simulations Jetring512, Jetring1024dz and Jetring1024drdz at increasing mesh resolution. The convergence of the initial turbulence and shear-layer properties with respect to the grid is also examined from the solutions computed in Jetring1024drdz2δ_θ on the grid of Jetring1024drdz for the jet with a thicker initial shear layer.

A. Initial conditions

The properties of the initial turbulence in the shear layers are characterized by calculating spectra of the fluctuating axial velocity just downstream of the pipe lip at $r = r_0$ and at $z = 22\delta_\theta(0)$, that is to say at $z = 0.4r_0$ in Jetring512, Jetring1024dz and Jetring1024drdz and at $z = 0.8r_0$ in Jetring1024drdz2δ_θ.

The frequency spectra thus determined are represented in figure 2(a) as functions of the Strouhal number $\mathrm{St}_\theta = f\delta_\theta(0)/u_j$. Despite slight changes in magnitude probably due to different flow developments between $z = 0$ and $z = 0.4r_0$, the spectra from Jetring512, Jetring1024dz and Jetring1024drdz display very similar shapes, indicating that the distribution of the frequency components of the jet initial disturbances does not

vary much with the grid. They also agree reasonably well with the spectrum from Jetring1024drdz2δ_θ, which suggests a fair grid convergence.

The azimuthal spectra of axial velocity computed at $r = r_0$ and at $z = 22\delta_\theta(0)$ are shown in figures 2(b) as functions of the normalized wave number $k_\theta\delta_\theta(0)/r_0$. Those from Jetring512, Jetring1024dz and Jetring1024drdz exhibit similar smooth shapes, with peak components at $k_\theta\delta_\theta(0)/r_0 \simeq 0.7$ in Jetring512 and Jetring1024dz, and at $k_\theta\delta_\theta(0)/r_0 \simeq 0.8$ in Jetring1024drdz. The origin of the dominant wave numbers in the azimuthal spectra remains unclear, but they do not seem strongly related to the discretization. The azimuthal spectra from Jetring1024drdz and Jetring1024drdz2δ_θ indeed appear nearly superimposed over a wide range of wavenumbers, which supports that this initial flow feature is grid-independent in Jetring1024drdz.

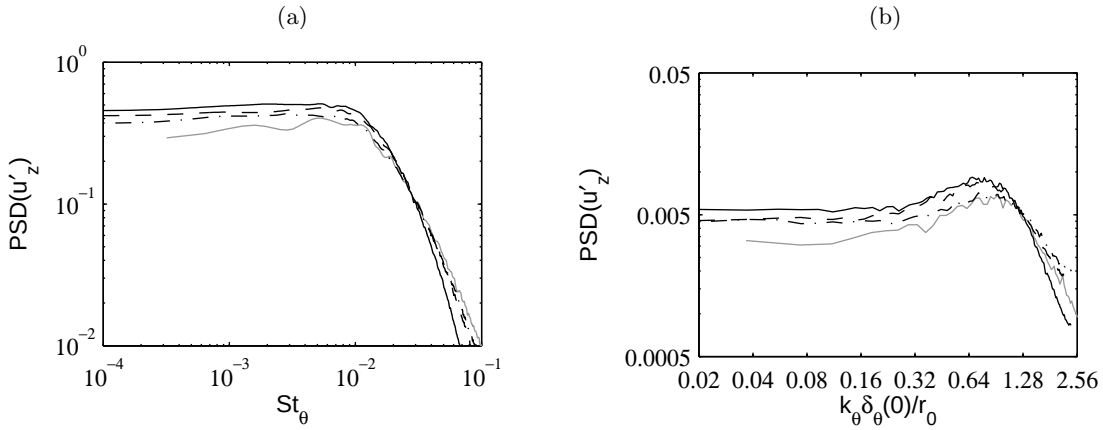

Figure 2. Power spectral densities (PSD) normalized by u_j of fluctuating velocity u'_z at $r = r_0$ and $z = 22\delta_\theta(0)$, as functions (a) of $\mathrm{St}_\theta = f\delta_\theta(0)/u_j$ and (b) of $k_\theta\delta_\theta(0)/r_0$, for ——— Jetring512, − − − Jetring1024dz, − · − · Jetring1024drdz, ——— Jetring1024drdz2δ_θ.

B. Aerodynamic fields

1. *Shear-layer development*

Snapshots of the vorticity norm obtained from $z = 0$ to $z = 3r_0$ in the (z, r) plane in Jetring512, Jetring1024dz and Jetring1024drdz are first presented in figure 3 to illustrate the shear-layer development downstream of the nozzle lip. As expected for initially turbulent jets, vortical structures are found immediately at the exit section. Both small and large structures are also observed in agreement with the Reynolds number $\mathrm{Re}_D = 10^5$. A wider range of fine turbulent scales is however noticed in the simulations using finer grids.

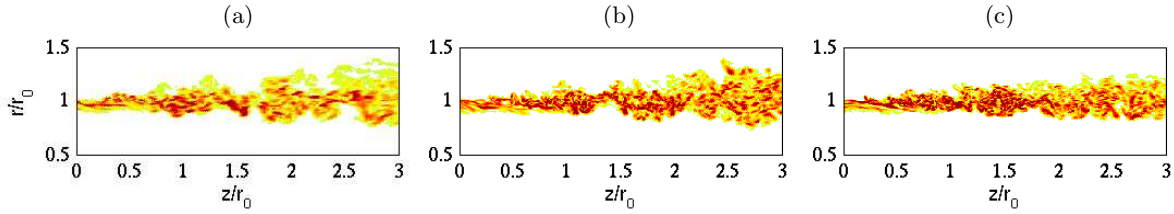

Figure 3. Snapshots in the (z, r) plane of vorticity norm in the shear layers just downstream of the pipe lip: (a) Jetring512, (b) Jetring1024dz, (c) Jetring1024drdz. The colour scales range up to the level of $25u_j/r_0$.

A vorticity snapshot obtained from Jetring1024drdz2δ_θ for the jet with a double initial shear-layer thickness is now shown in figure 4, and compared with a vorticity snapshot from Jetring1024drdz using $x/\delta_\theta(0)$-y/r_0 coordinates. It should be borne in mind that the same grid is used in the two cases to study grid convergence. It is however limited to $z = 8r_0$, *i.e.* $z \simeq 225\delta_\theta(0)$, in Jetring1024drdz2$\delta_\theta$. In the figure, the doubling of the shear-layer thickness in Jetring1024drdz2δ_θ appears clearly. The mixing layers also show a wide range of turbulent scales in both simulations.

The variations of the jet shear-layer momentum thickness are represented in figure 5. They are normalized by $\delta_\theta(0)$, and plotted up to $z = 225\delta_\theta(0)$, that is $z = 4r_0$ in Jetring512, Jetring1024dz and Jetring1024drdz, and $z = 8r_0$ in Jetring1024drdz2δ_θ. The mixing layers are found to spread more slowly as the grid resolution

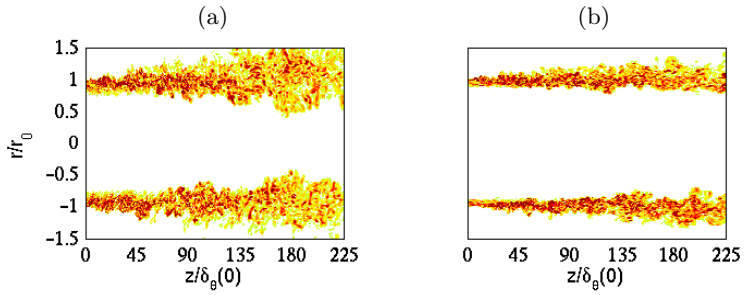

Figure 4. Snapshots in the (z, r) plane of vorticity norm from (a) Jetring1024drdz2δ_θ and (b) Jetring1024drdz. The z-axis is normalized by $\delta_\theta(0)$. The colour scales range up to the level of (a) $11.25u_j/r_0$ and (b) $15u_j/r_0$.

gradually increases. More spectacularly, the profiles obtained from Jetring1024drdz and Jetring1024drdz2δ_θ using the finest mesh grid can hardly be distinguished from each other. This demonstrates that grid convergence is achieved in Jetring1024drdz for the mean development of the mixing layer.

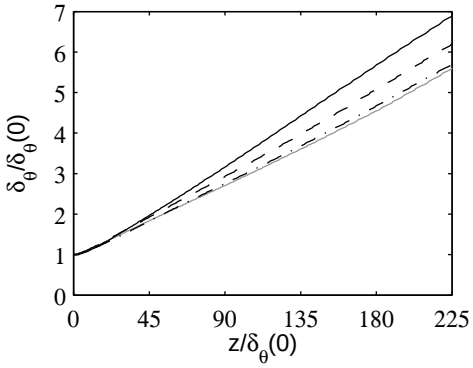

Figure 5. Variations of shear-layer momentum thickness $\delta_\theta/\delta_\theta(0)$, as functions of $z/\delta_\theta(0)$, for ——— Jetring512, − − − Jetring1024dz, − · − · Jetring1024drdz, ——— Jetring1024drdz2δ_θ.

The profiles of the peak rms values of u'_z, u'_r and u'_θ and of the peak magnitudes of Reynolds shear stress $< u'_r u'_z >$ are plotted in figure 6 as functions of $z/\delta_\theta(0)$, up to $z = 225\delta_\theta(0)$ as previously. In Jetring1024drdz, as the radial resolution at $r = r_0$ is doubled with respect to that in Jetring1024dz, the turbulence intensities are found to increase more slowly with the axial position, with maximum values moving from $< u'^2_z >^{1/2} = 0.157u_j$ and $< u'^2_r >^{1/2} = 0.117u_j$ in Jetring1024dz down to $< u'^2_z >^{1/2} = 0.130u_j$ and $< u'^2_r >^{1/2} = 0.112u_j$ in Jetring1024drdz. In the latter simulation, the rms velocity levels even grow nearly monotonically, in the same way as measured in initially turbulent axisymmetric mixing layers.[31] They are also similar to those obtained from Jetring1024drdz2δ_θ at a double resolution, which indicates that they are practically grid-converged. The mixing-layer flow solutions from Jetring1024drdz can therefore be regarded as trustworthy.

These results are in agreement with the analyses of LES reliability conducted in another paper.[2] In that paper, the LES mesh grids are indeed found to provide suitable axial and radial mixing-layer discretizations in Jetring1024dz and Jetring1024drdz, but not in Jetring512. The radial grid resolution might however be low in Jetring1024dz, whereas it can be expected to be sufficient in Jetring1024drdz. The physical relevance of the LES fields in Jetring1024drdz is also discussed, and molecular viscosity is shown to be the dominant dissipation mechanism for the scales discretized at least by 7 points per wavelength in the shear layers. The dynamics of the coherent structures developing in Jetring1024drdz should consequently not be significantly affected by undesirable dissipation.

Spectra of the radial velocity, computed along the lip line at $z = 83\delta_\theta(0)$ and $166\delta_\theta(0)$ (*i.e.* at $z = 1.5r_0$ and $3r_0$ in Jetring512, Jetring1024dz and Jetring1024drdz, and at $z = 3r_0$ and $6r_0$ in Jetring1024drdz2δ_θ), are finally represented in figure 7 as functions of $\mathrm{St}_\theta = f\delta_\theta(0)/u_j$. They all display broadband shapes, especially with respect to spectra obtained in initially laminar jets,[16] and maximum levels for similar St_θ. The highest components are more precisely found around $\mathrm{St}_\theta = 0.013$ at $z = 83\delta_\theta(0)$, and $\mathrm{St}_\theta = 0.0065$ at $z = 166\delta_\theta(0)$. The former frequency is typical of frequencies originally dominating in annular mixing layers,[32]

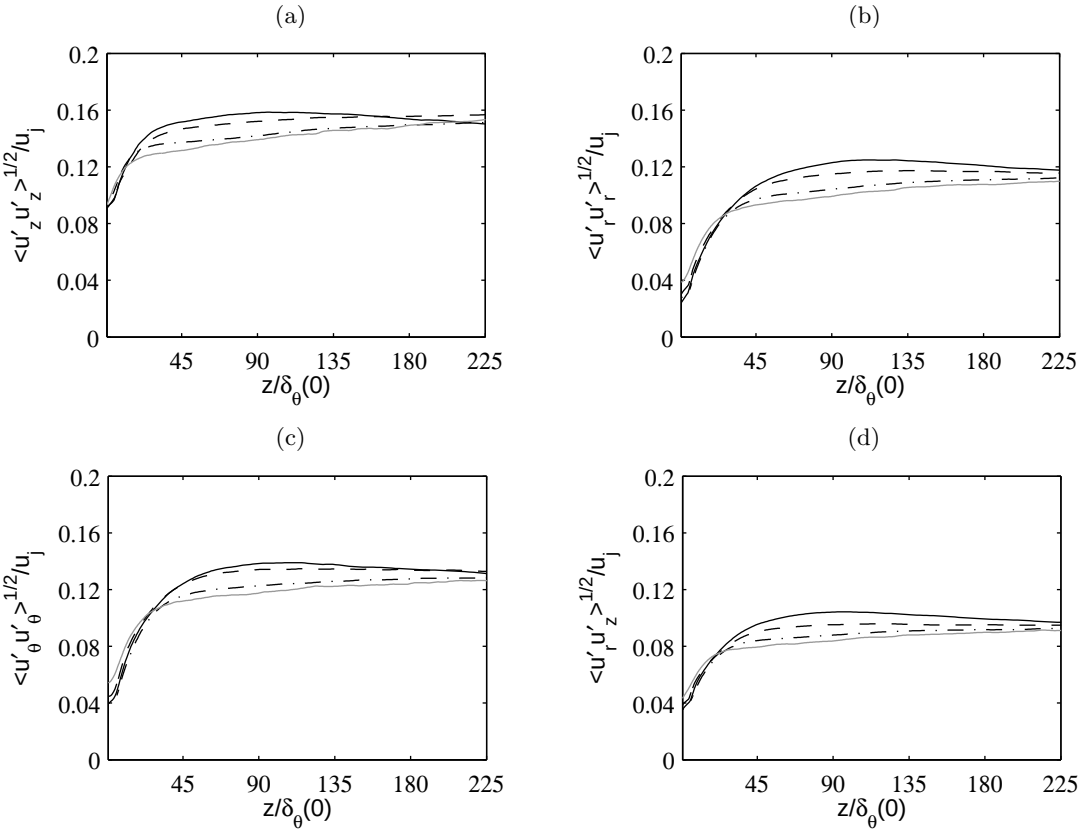

Figure 6. Variations of the peak rms values of velocities (a) u'_z, (b) u'_r and (c) u'_θ, and (d) of the peak magnitudes of Reynolds shear stress $< u'_r u'_z >$, as functions of $z/\delta_\theta(0)$, for ——— Jetring512, − − − Jetring1024dz, − · − · Jetring1024drdz, ——— Jetring1024drdz2δ_θ.

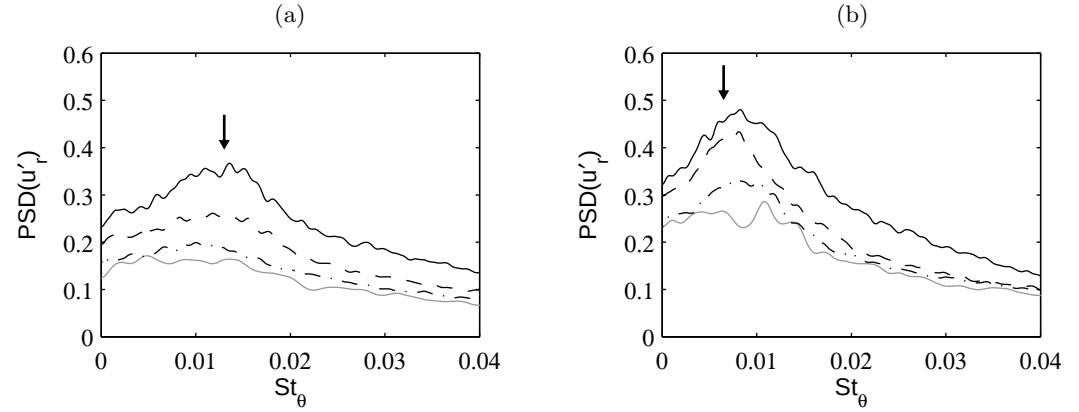

Figure 7. Power spectral densities (PSD) normalized by u_j of radial velocity u'_r, (a) at $r = r_0$ and $z = 83\delta_\theta(0)$ and (b) at $r = r_0$ and $z = 166\delta_\theta(0)$, as functions of $St_\theta = f\delta_\theta(0)/u_j$, for ——— Jetring512, − − − Jetring1024dz, − · − · Jetring1024drdz, ——— Jetring1024drdz2δ_θ. The arrows indicate (a) $St_\theta = 0.013$ and (b) $St_\theta = 0.0065$.

which suggests the presence of a first stage of coherent vortex pairings. Their strengths are rather limited and decrease with the grid resolution. They seem nonetheless persistent. This claim is particularly supported by the fairly good comparison between the spectra from Jetring1024drdz and those from Jetring1024drdz2δ_θ, for a shear layer at the same Re_θ with a double initial thickness.

2. *Jet flow development*

Vorticity snapshots obtained up to $z = 25r_0$ in Jetring512, Jetring1024dz and Jetring1024drdz are shown in figure 8. Similar jet turbulent developments are found. In all cases, in particular, the end of the jet potential core appears located around 15 radii downstream of the pipe-nozzle exit.

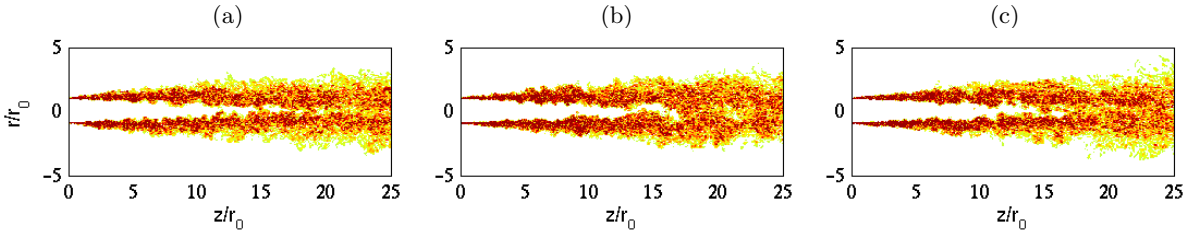

Figure 8. Snapshots in the (z, r) plane of vorticity norm in the full jets up to $z = 25r_0$: (a) Jetring512, (b) Jetring1024dz, (c) Jetring1024drdz. The colour scales range up to the level of $5u_j/r_0$.

The variations of the mean and rms values of the axial velocity along the jet centerline are presented in figure 9. In figure 9(a), the length of the potential core is seen to vary from $z_c = 15.2r_0$ in Jetring1024dz up to $z_c = 16.4r_0$ in Jetring512, where $< u_z > (z = z_c) = 0.95u_j$. The jets also appear to spread more rapidly in Jetring1024dz and Jetring1024drdz than in Jetring512. In figure 9(b), the rms values of velocity u'_z on the jet axis also change when finer grids are used. They are indeed significantly higher in Jetring1024dz and Jetring1024drdz. This leads, for instance, to rms axial velocity values at $r = 0$ and $z = z_c$, at the end of the potential core, of $0.067u_j$ in Jetring512 but of $0.082u_j$ in Jetring1024dz.

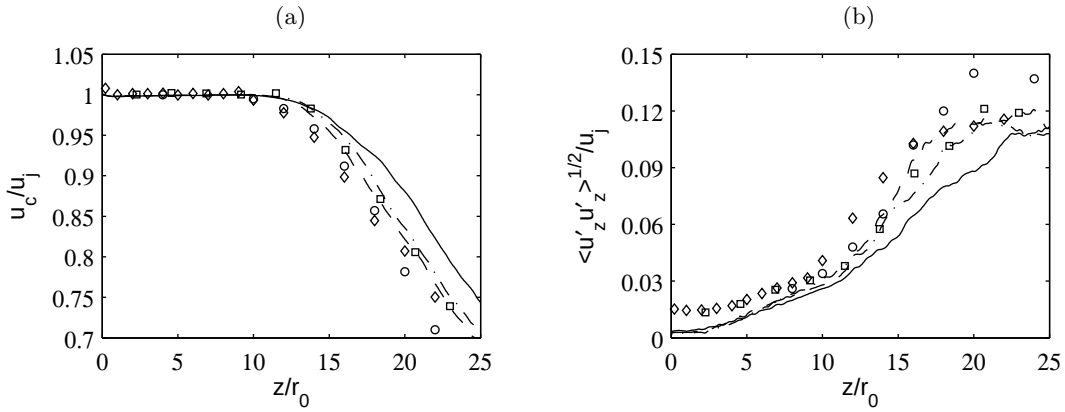

Figure 9. Variations (a) of centerline mean axial velocity u_c and (b) of centerline rms values of velocity u'_z, for ——— Jetring512, − − − Jetring1024dz, − · − · Jetring1024drdz. Measurements for Mach 0.9 jets at $\mathrm{Re}_D \geq 5 \times 10^5$: ○ Lau *et al.*,[33] □ Arakeri *et al.*,[34] ◇ Fleury *et al.*[35]

Experimental data provided by Lau *et al.*,[33] Arakeri *et al.*,[34] and Fleury *et al.*[35] for Mach number 0.9 jets at $\mathrm{Re}_D \geq 5 \times 10^5$, all probably containing significant nozzle-exit turbulence, are also shown in figure 9. It is interesting to note here that the use of higher grid resolution in Jetring1024dz and Jetring1024drdz results in centerline mean and rms velocity profiles in better agreement with these measurements.

C. Acoustic fields

Snapshots of the near-field fluctuating pressure obtained in Jetring512, Jetring1024dz and Jetring1024drdz are presented in figure 10. The pressure fields appear rather clean, no acoustic radiation being in particular clearly noticed from the pipe exit. Sound waves are also visibly coming from the flow region located around $z = 2.5r_0$, where the shear-layer transition takes place. Their origin will be discussed in what follows.

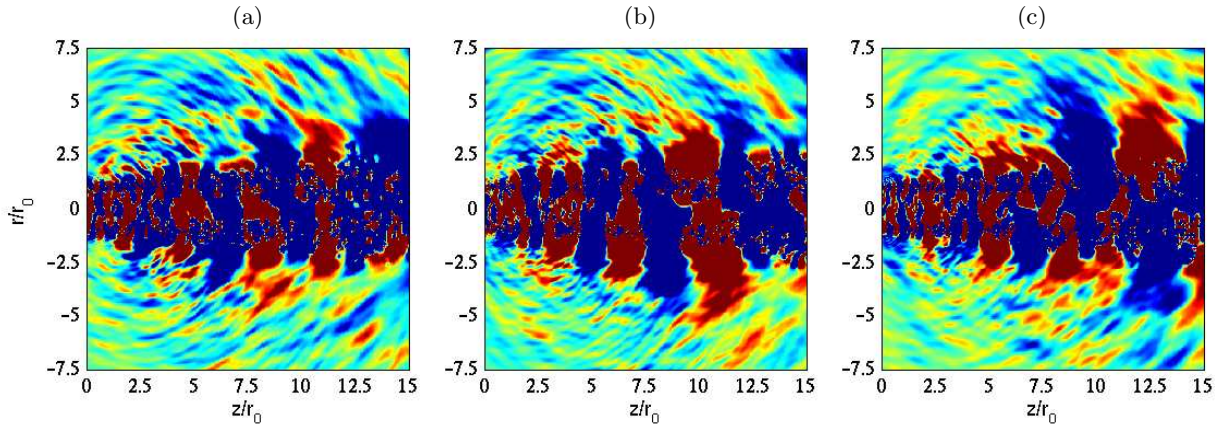

Figure 10. Snapshots in the (z, r) plane of fluctuating pressure: (a) Jetring512, (b) Jetring1024dz, (c) Jetring1024drdz. The colour scale ranges from levels of -100 Pa to 100 Pa.

The pressure spectra estimated at $60r_0$ from the nozzle exit at the angles $\phi = 40^o$ and 90^o relative to the jet direction are represented in figure 11. For Strouhal numbers $\mathrm{St}_D \leq 0.5$, compared to experimental data obtained for jets at Reynolds numbers higher than 7.8×10^5, noise components are lower in Jetring512, but they rather agree in Jetring1024dz and Jetring1024drdz. For $\mathrm{St}_D \geq 0.5$, additional humps appear with respect to the measurements in all cases. These humps are approximately centered around $\mathrm{St}_D = 0.072$, or equally $\mathrm{St}_\theta = 0.0065$ here. This St_θ value suggests that they are associated with a first stage of vortex pairings in the mixing layers. This link is further supported by the fact that this frequency is also close to half of the peak frequencies in the velocity spectra calculated at $r = r_0$ and $z = 1.5r_0$, shown in figure 7(a).

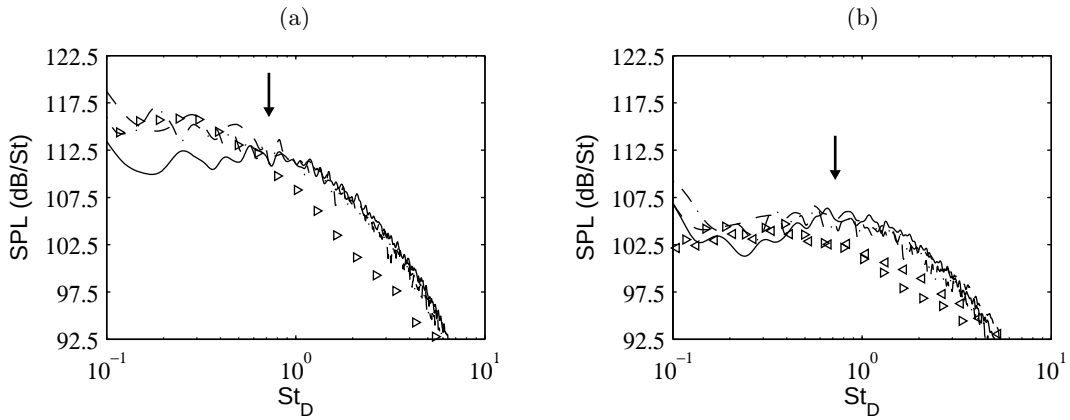

Figure 11. Sound pressure levels (SPL) at $60r_0$ from the jet exit, as functions of $\mathrm{St}_D = fD/u_j$, at the angles of (a) 40^o and (b) 90^o, for ——— Jetring512, − − − Jetring1024dz, − · − · Jetring1024drdz. The arrows indicate the frequency determined using $\mathrm{St}_\theta = f\delta_\theta(0)/u_j = 0.0065$. Measurements for jets at $\mathrm{Re}_D \geq 7.8 \times 10^5$: ◁ Tanna,[36] ▷ Bogey *et al.*[37]

The components attributed to vortex pairings in the sound spectra appear persistent regardless of the grid. Since they do not appreciably differ in Jetring512 and in Jetring1024drdz using twice-as-fine discretizations in every grid direction, they are even unlikely to be significantly affected by an extra increase of the resolution. The generation of vortex-pairing noise in the present jet can thus be expected to result from physical reasons such as insufficient initial turbulence levels[3] and/or relatively moderate Reynolds numbers Re_D and Re_θ, for instance.

IV. Conclusion

In the present paper, compressible LES of an initially nominally turbulent jet at Mach number 0.9 and Reynolds number 10^5, whose boundary layers are tripped inside a pipe nozzle, are presented. The results obtained from the simulation at highest resolution, using a 252 million point grid with minimum radial,

azimuthal and axial mesh spacings equal, respectively, to 0.20, 0.34 and 0.40 times the exit boundary-layer momentum thickness, appear numerically accurate as well as physically relevant. This is supported by a grid-convergence study involving the simulation of a jet with a thicker initial shear layer, and by *a posteriori* assessments of the LES quality.[2] The mean and turbulent flow fields from the LES using the finest grid are moreover found to agree well with what is expected in initially turbulent jets at high Reynolds number, in particular in terms of potential core length and of the growth of peak turbulence intensities downstream of the nozzle lip. A noise component apparently caused by coherent vortex pairings in the mixing layers is also observed. Its persistence in jets containing stronger initial turbulence levels[3] or at higher Reynolds numbers will be examined in future works.

Acknowledgments

This work was granted access to the HPC resources of the Institut du Développement et des Ressources en Informatique Scientifique (IDRIS) under the allocation 2010-020204 made by GENCI (Grand Equipement National de Calcul Intensif).

References

[1]Bogey, C., Marsden, O., and Bailly, C., "Flow and acoustic fields of Reynolds number 10^5, subsonic jets with tripped exit boundary layers," AIAA Paper 2010-3727.

[2]Bogey, C., Marsden, O., and Bailly, C., "Large-Eddy Simulation of the flow and acoustic fields of a Reynolds number 10^5 subsonic jet with tripped exit boundary layers," *Phys. Fluids*, Vol. 3, No. 3, 2011, 035104.

[3]Bogey, C., Marsden, O. and Bailly, C., "A computational study of the effects of nozzle-exit turbulence level on the flow and acoustic fields of a subsonic jet," *17th AIAA/CEAS Aeroacoustics Conference*, 6-8 June 2011, Portland, Oregon, USA.

[4]Colonius, T. and Lele, S.K., "Computational aeroacoustics: progress on nonlinear problems of sound generation," *Progress in Aerospace Sciences*, Vol. 40, 2004, pp. 345-416.

[5]Bogey, C. and Bailly, C., "Contributions of CAA to jet noise research and prediction," *Int. J. Comput. Fluid Dyn.*, Vol. 18, No. 6, 2004, pp. 481-491.

[6]Wang, M., Freund J.B., and Lele, S.K., "Computational prediction of flow-generated sound," *Annu. Rev. Fluid. Mech.*, Vol. 38, 2006, pp. 483-512.

[7]Hill, W.G., Jenkins, R.C., and Gilbert, B.L., "Effects of the initial boundary-layer state on turbulent jet mixing," *AIAA J.*, Vol. 14, No. 11, 1976, pp. 1513-1514.

[8]Hussain, A.K.M.F. and Zedan, M.F., "Effects of the initial condition on the axisymmetric free shear layer: Effects of the initial fluctuation level," *Phys. Fluids*, Vol. 21, No. 9, 1978, pp. 1475-1481.

[9]Crighton, D.G., "Acoustics as a branch of fluid mechanics," *J. Fluid Mech.*, Vol. 106, 1981, pp. 261-298.

[10]Hussain, A.K.M.F., "Coherent structures–reality and myth," *Phys. Fluids*, Vol. 26, No. 10, 1983, pp. 2816-2850.

[11]Zaman, K.B.M.Q., "Far-field noise of a subsonic jet under controlled excitation," *J. Fluid Mech.*, Vol. 152, 1985, pp. 83-111.

[12]Zaman, K.B.M.Q., "Effect of initial condition on subsonic jet noise," *AIAA J.*, Vol. 23, 1985, pp. 1370-1373.

[13]Bridges, J.E. and Hussain, A.K.M.F., "Roles of initial conditions and vortex pairing in jet noise," *J. Sound Vib.*, Vol. 117, No. 2, 1987, pp. 289-311.

[14]Bogey, C., Barré, S., and Bailly, C., "Direct computation of the noise generated by subsonic jets originating from a straight pipe nozzle," *Int. J. of Aeroacoustics*, Vol. 7, No. 1, 2008, pp. 1-22.

[15]Uzun, A. and Hussaini, M., "Investigation of high frequency noise generation in the near-nozzle region of a jet using large eddy simulation," *Theoret. Comput. Fluid Dynamics*, Vol. 21, No. 4, 2007, pp. 291-321.

[16]Bogey, C. and Bailly, C., "Influence of nozzle-exit boundary-layer conditions on the flow and acoustic fields of initially laminar jets," *J. Fluid Mech.*, Vol. 663, 2010, pp. 507-539

[17]Maestrello, L. and McDaid, E., "Acoustic characteristics of a high-subsonic jet," *AIAA J.*, Vol. 9, No. 6, 1971, pp. 1058-1066.

[18]Batt, R.G., "Some measurements on the effect of tripping the two-dimensional shear layer," *AIAA J.*, Vol. 13, No. 2, 1975, pp. 245-247.

[19]Morris, P.J. and Zaman, K.B.M.Q., "Velocity measurements in jets with application to noise source modelling," *J. Sound Vib.*, Vol. 329, No. 4, 2009, pp. 394-414.

[20]Mohseni, K. and Colonius, T., "Numerical treatment of polar coordinate singularities," *J. Comput. Phys.*, Vol. 157, No. 2, 2000, pp. 787-795.

[21]Bogey, C. and Bailly, C., "A family of low dispersive and low dissipative explicit schemes for flow and noise computations," *J. Comput. Phys.*, Vol. 194, No. 1, 2004, pp. 194-214.

[22]Bogey, C., de Cacqueray, N., and Bailly, C., "Finite differences for coarse azimuthal discretization and for reduction of effective resolution near origin of cylindrical flow equations," *J. Comput. Phys.*, Vol. 230, No. 4, 2011, pp. 1134-1146.

[23]Bogey, C., de Cacqueray, N., and Bailly, C., "A shock-capturing methodology based on adaptative spatial filtering for high-order non-linear computations," *J. Comput. Phys.*, Vol. 228, No. 5, 2009, pp. 1447-1465.

[24]Berland, J., Bogey, C., Marsden, O., and Bailly, C., "High-order, low dispersive and low dissipative explicit schemes for multi-scale and boundary problems," *J. Comput. Phys.*, Vol. 224, No. 2, 2007, pp. 637-662.

[25]Bogey, C. and Bailly, C., "Large Eddy Simulations of transitional round jets: influence of the Reynolds number on flow development and energy dissipation," *Phys. Fluids*, Vol. 18, No. 6, 2006, 065101.

[26]Bogey, C. and Bailly, C., "Large eddy simulations of round jets using explicit filtering with/without dynamic Smagorinsky model," *Int. J. Heat and Fluid Flow*, Vol. 27, No. 4, 2006, pp. 603-610.

[27]Bogey, C. and Bailly, C., "Turbulence and energy budget in a self-preserving round jet: direct evaluation using large-eddy simulation," *J. Fluid Mech.*, Vol. 627, 2009.

[28]Tam, C.K.W and Dong, Z., "Radiation and outflow boundary conditions for direct computation of acoustic and flow disturbances in a nonuniform mean flow., *J. Comput. Acoust.*, Vol. 4, No. 2,, 1996, pp. 175201.

[29]Bogey, C. and C. Bailly, C., "Three-dimensional non reflective boundary conditions for acoustic simulations: far-field formulation and validation test cases," *Acta Acustica*, Vol. 88, No. 4, 2002, pp. 463-471.

[30]Bogey, C., Barré, S., Juvé, D., and Bailly, C., "Simulation of a hot coaxial jet : direct noise prediction and flow-acoustics correlations," *Phys. Fluids*, Vol. 21, No. 3, 2009, 035105.

[31]Husain, Z.D. and Hussain, A.K.M.F., "Axisymmetric mixing layer: influence of the initial and boundary conditions," *AIAA J.*, Vol. 17, No. 1, 1979, pp. 48-55.

[32]Gutmark, E. and Ho, C.-M., "Preferred modes and the spreading rates of jets," *Phys. Fluids*, Vol. 26, No. 10, 1983, pp. 2932-2938.

[33]Lau, J.C., Morris, P.J., and Fisher, M.J., "Measurements in subsonic and supersonic free jets using a laser velocimeter," *J. Fluid Mech.*, Vol. 93, No. 1, 1979, pp. 1-27.

[34]Arakeri, V.H., Krothapalli, A., Siddavaram, V., Alkislar, M.B., and Lourenco, L., "On the use of microjets to suppress turbulence in a Mach 0.9 axisymmetric jet," *J. Fluid Mech.*, Vol. 490, 2003, pp. 75-98.

[35]Fleury, V., Bailly, C., Jondeau, E., Michard, M., and Juvé, D., "Space-time correlations in two subsonic jets using dual-PIV measurements," *AIAA J.*, Vol. 46, No. 10, 2008, pp. 2498-2509.

[36]Tanna, H.K., "An experimental study of jet noise. Part I: Turbulent mixing noise," *J. Sound Vib.*, Vol. 50, No. 3, 1977, pp. 405-428.

[37]Bogey, C., Barré, S., Fleury, V., Bailly, C., and Juvé, D., "Experimental study of the spectral properties of near-field and far-field jet noise," *Int. J. of Aeroacoustics*, Vol. 6, No. 2, 2007, pp. 73-92.